

Journal of
Applied Remote Sensing

RemoteSensing.SPIEDigitalLibrary.org

**Hourly turbidity monitoring using
Geostationary Ocean Color Imager
fluorescence bands**

Ruhul Amin
Igor Shulman

Hourly turbidity monitoring using Geostationary Ocean Color Imager fluorescence bands

Ruhul Amin^{a,*} and Igor Shulman^b

^aBioOptoSense LLC, 4007 Prytania Street, New Orleans, Louisiana 70115, United States
^bStennis Space Center, Naval Research Laboratory, Code 7331, Mississippi 39529, United States

Abstract. The Geostationary Ocean Color imager (GOCI) is the first geostationary ocean color satellite sensor that collects hourly images eight times per day during daylight. This high frequency image acquisition makes it possible to study more detailed dynamics of red tide blooms, sediment plumes, and colored dissolved organic matter plumes, and can aid in the prediction of biophysical phenomena. We apply the red band difference and the fluorescence line height algorithms to GOCI imagery to separate waters with high algal and nonalgal particles and validate the results with the MODIS imagery. We also track optical features using hourly GOCI imagery and assess their movement through comparisons with predicted ocean currents derived from the navy coastal ocean model and tidal data. © *The Authors. Published by SPIE under a Creative Commons Attribution 3.0 Unported License. Distribution or reproduction of this work in whole or in part requires full attribution of the original publication, including its DOI.* [DOI: [10.1117/1.JRS.9.096024](https://doi.org/10.1117/1.JRS.9.096024)]

Keywords: geostationary satellite; ocean color remote sensing; coastal dynamics; optical and bio-optical features.

Paper 15056 received Jan. 20, 2015; accepted for publication Jun. 22, 2015; published online Aug. 4, 2015.

1 Introduction

The Geostationary Ocean Color Imager (GOCI) is one of the three payloads of the Korean Communication, Ocean and Meteorological Satellite (COMS) that was successfully launched in June 2010 from the Space Center in Kourou, French Guiana, by the Ariane 5 Launch Vehicle.^{1,2} GOCI is the world's first geostationary ocean color sensor designed with visible and near-infrared (NIR) bands that can measure radiance from the ocean surface. The advantage of GOCI is that it can obtain images every hour during the day which facilitates monitoring the ocean in near real time. GOCI consists of 16 (4×4) slot images covering 2500×2500 km² around the Korean Peninsula centered at 36°N and 130°E with a roughly 500-m spatial resolution.^{1,2} The sensor also has a very high signal-to-noise ratio (over 1000:1), which is necessary for detection of very low ocean radiances.^{1,2} GOCI has six visible bands centered at 412, 443, 490, 555, 660, and 680 nm, and two NIR bands centered at 745 and 865 nm.^{1,2} The expected operational life expectancy of the GOCI mission is about 7 years.^{1,2}

Polar-orbiting satellite sensors such as the Moderate Resolution Imaging Spectroradiometer (MODIS) and the Medium Resolution Imaging Spectrometer (MERIS) have been widely used for ocean color studies.^{3,4} However, those sensors have limitations in monitoring dynamic variation such as daily or hourly variations of the ocean surface. These sensors typically collect one image per day at about 1 km resolution. While these sensors provide an enormous advantage in terms of spatial coverage, cloud coverage is a serious restriction. Daily revisit time is another limitation for these sensors, particularly in optically complex coastal waters with high temporal variability due to tides, wind-driven advection, resuspension, and so on. For these reasons, geostationary sensors with high temporal frequency observations are critical for studying and quantifying biological and physical processes within the coastal ocean. Unlike polar-orbiting satellites which provide only one or two images of the same geographic area per day, GOCI collects images every hour from 00:00 GMT to 07:00 GMT (totaling eight images per day).

*Address all correspondence to: Ruhul Amin, E-mail: biooptosense@gmail.com

This high frequency image acquisition makes it possible to study more detailed time series analyses and movements of red tide blooms, sediment and colored dissolved organic matter (CDOM) plumes and can aid in the prediction of biophysical phenomena.

Phytoplankton blooms develop over the course of a few days to a week and the complete dynamics of the blooms are not always captured by individual polar-orbiting satellite sensors. The physiology of phytoplankton cells (chlorophyll content, nutrient uptake, and so on) varies with diel cycles, and this has a significant impact on their growth rate and hence, their primary production.⁵ Thus, multiple observations per day over several days would permit more robust satellite-based estimates of primary production. However, for such estimations, we need more reliable atmospheric correction, particularly for the coastal ocean where standard NIR atmospheric correction⁶ often fails due to higher turbidity and significantly higher radiance contributions to the NIR bands. Since the water-leaving radiance at NIR can no longer be considered negligible for the use of atmospheric correction over turbid waters,⁷ negative readings may result in the blue-green bands due to atmospheric overcorrection.^{8,9} Algorithms that use blue-green bands^{10–12} usually perform poorly in coastal waters due to increased absorption of CDOM, increased particle scattering, inaccurate atmospheric correction, and shallow bottom reflectance.^{13–16} Because of these uncertainties, it is often very challenging to accurately identify optical and bio-optical features using these algorithms. Thus, algorithms less sensitive to atmospheric correction are desirable.

Although GOCI is the first geostationary ocean color sensor, the geostationary Spinning Enhanced Visible and InfraRed Imager meteorological sensor has been used to map suspended particulate matter (SPM) in turbid coastal waters.¹⁷ This sensor is limited, however, with just a single broad red band and an NIR band used for SPM estimation. GOCI also has been used to map turbidity around the coastal region of the Korean Peninsula.^{1,18} Unlike other studies,^{1,17,18} we use the red band difference (RBD) and fluorescence line height (FLH) algorithms, which are less sensitive to atmospheric corrections and CDOM absorption, to reduce uncertainties.

The objective of this study was to test the feasibility of separating algal and nonalgal components using GOCI imagery, and to determine whether high frequency dynamics can be detected. We also attempted to track the features using hourly GOCI imagery and assess their movement through comparisons with predicted ocean currents derived from the navy coastal ocean model (NCOM). Since MODIS RBD and FLH results have been validated,^{3,4} we used MODIS to validate GOCI results and then assess the high frequency dynamics from the hourly imageries in the coastal waters of the Korean Peninsula.

2 Materials and Methods

2.1 Satellite Data

We acquired all eight GOCI L1B hourly data for April 5, 2011, through the Naval Oceanographic Office and the corresponding MODIS-aqua L1B data from NASA LAADS Web.¹⁹ To reduce uncertainties from the illumination and viewing geometries, we excluded first (at 00:16 GMT) and last (at 07:00 GMT) GOCI imageries from our analysis. We used the standard GOCI data processing software system that consists of both the image processing system (IMPS) and the GOCI data processing system (GDPS).^{2,20} The IMPS is used to generate level 1B data from the raw data, whereas the GDPS is used with level 1B data to generate processed level 2 data. Level 2 data are generated with cloud and land masking, atmospheric correction, bidirectional correction, and ocean color product retrievals. GOCI level 2 data consist of water-leaving radiance (L_w), normalized water-leaving radiance (nL_w), chlorophyll concentration, total suspended sediment concentration, and many other ocean color products. GDPS also generates level 3 data which consist of fishery information, primary productivity, water quality level, and water current vectors.²¹ However, in this study, we only used the standard GDPS^{2,20} (version 1.2) processed GOCI nL_w in the red and NIR regions since FLH and RBD use radiance/reflectance in these bands.

We processed MODIS-aqua data through the automated processing system (APS)²² that used the standard NASA atmospheric correction algorithm.⁶ APS was developed by the Naval Research Laboratory (NRL) at Stennis Space Center (NRL/SSC) which produces daily ocean

color products from real time or archived data from sensors such as the visible infrared imaging radiometer suite (VIIRS), MODIS, MERIS, and GOCI.²² It is a powerful, extendable, image-processing tool which is a complete end-to-end system including sensor calibration, atmospheric correction and bio-optical inversion. APS incorporates, and is consistent with, the latest NASA SeaWiFS Data Analysis System (SeaDAS) code and enables us to produce the NASA standard MODIS products as well as navy-specific products using NRL algorithms.²² APS operates in a stand-alone batch processing mode, which facilitates testing and validation of new products and algorithms, and reprocessing of many data files (dozens of scenes/day). Furthermore, APS can automatically extract image data from regions-of-interest to facilitate time series analyses and also match-ups with *in situ* data for a specific location. NRL/SSC is one of only a few institutions that has digested and implemented complete MODIS, VIIRS, and GOCI processing codes while maintaining compatibility with NASA/Goddard SeaDAS products.

2.2 Navy Coastal Ocean Model

The NCOM model is a primitive-equation, three-dimensional (3-D), hydrostatic model. It uses the Mellor–Yamada level 2.5 turbulence closure scheme and the Smagorinsky formulation for horizontal mixing.²³ The model is set up at 3-km horizontal resolution and 50 vertical layers around the Korean Peninsula. The model was initialized on 00 GMT April 1, 2011, with sea surface height, temperature, salinity, and velocities data derived from the 1/8 deg horizontal resolution NCOM global model.^{24,25} The model was forced with surface fluxes from the navy global atmospheric prediction system (NOGAPS).²⁶ Open boundary conditions for the NCOM model are derived from the NCOM global model. Tidal forcing is introduced by using tidal sea surface height and velocities at the model open boundaries from the Oregon State University tidal model.²⁷ Eight tidal constituents (M2, S2, N2, K2, K1, O1, P1, and Q1) were used. For the assimilation of physical observations (temperature and salinity), the NCOM ICON model uses the navy coupled ocean data assimilation (NCODA) system.^{28,29} The NCODA is a fully 3-D multivariate optimum interpolation system. Assimilation of temperature and salinity data is performed every 12 hours (assimilation cycle). The NCODA assimilates satellite altimeter observations and satellite surface temperature, as well as available *in situ* vertical temperature and salinity profiles from expendable bathythermographs, ARGO floats, moored buoys, and gliders from the global ocean data assimilation experiment dataset. The datasets, processing and quality control procedures are described in Refs. 28 and 29. Results of glider, ship and satellite data assimilation into the NCOM model for the Monterey Bay area are described in Refs. 30 and 31.

2.3 Algorithms

The RBD algorithm was developed for relatively low backscattering blooms such as dinoflagellates^{3,4} by taking advantage of the chlorophyll fluorescence emission centered on 685 nm. Since there is nothing else in the water that fluoresces in the red region, the RBD easily identifies and separates chlorophyll rich regions from false chlorophyll-like features generated by CDOM plumes, sediment plumes and bottom reflectance. CDOM and sediments absorb light at blue wavelengths and bottom reflectance is typically observed at green wavelengths in optically shallow waters; therefore, the standard ocean color chlorophyll algorithms (such as OC3¹⁰) that are based on the blue/green radiance ratio can lead to erroneous chlorophyll estimates in coastal waters. On the other hand, the RBD algorithm is not affected by these water constituents. The RBD algorithm is expressed as follows:

$$\text{RBD} = nLw(\lambda_2) - nLw(\lambda_1), \quad (1)$$

where $nLw(\lambda)$ is the normalized water-leaving radiance which is defined as the upwelling radiance just above the sea surface in the absence of an atmosphere and with the sun directly overhead. The λ_1 is band 13 (667 nm) for MODIS and band 5 (660 nm) for GOCI, while the λ_2 is band 14 (678 nm) for MODIS and band 6 (680 nm) for GOCI. The RBD approach has been used to detect low backscattering algal blooms, particularly dinoflagellates, using MODIS and

MERIS imagery.^{34,32–34} In this study, the RBD approach was applied to GOCI imagery for the first time to detect relatively low backscattering blooms such as dinoflagellates, which are known to occur in the studied region.^{35–37} Since FLH cannot discriminate between bloom and sediment rich waters, we used FLH and RBD together to separate the two types of waters. The FLH products from GOCI were estimated using nLw at GOCI bands 5 (660 nm), 6 (680 nm), and 7 (745 nm) in a similar fashion as the MODIS FLH.³⁸

3 Physical and Bio-Optical Conditions During Geostationary Ocean Color Imager Surveys

The western coast of Korea, particularly around the urban estuary Gyeonggi Bay (Fig. 1), undergoes coastal erosion and geomorphologic changes near the tidal flats.³⁹ This sedimentary environment is influenced by the inland river systems and by the circulation of seawater due to tidal cycles.^{40–42} Gyeonggi Bay is a shallow (<40 m) semi-enclosed region located on the eastern part of the Yellow Sea.³⁹ This area has a large tidal range (4–8 m), strong tidal currents (1–2 m/s), and a large sediment supply (12.42×10^6 t/year) provided by the Han River.⁴³ We used the NCOM model currents to illustrate the dynamics in this region during the GOCI surveys. Figure 2 shows hourly current maps for April 5, 2011, from 01:00 GMT to 06:00 GMT. According to the model, around 01:00 GMT [Fig. 2(a)], 02:00 GMT [Fig. 2(b)], and 03:00 GMT [Fig. 2(c)], the current flows offshore, while around 04:00 GMT [Fig. 2(d)], the current appears to be reversing direction and starts flowing toward the coast [Fig. 2(e) at 05:00 GMT; Fig. 2(f) at 06:00 GMT]. Figure 2(g) shows the recorded tidal range for April 5, 2011, at Incheon (in Gyeonggi Bay at 37.4667° N and 126.5833° E) acquired from Ref. 44, where high tide was 8.89 m at 6:08 am local time (sunrise at 6:14 am), low tide was 1.14 m at 12:17 pm local time, and high tide was 8.47 m at 6:17 pm local time (sunset at 6:59 pm). Like the NCOM current, the tidal current changes direction around 03:00 GMT (noon local time) [Fig. 2(g)]. Based on the NCOM results and the tidal data (Fig. 2), we can see that the current was flowing offshore in

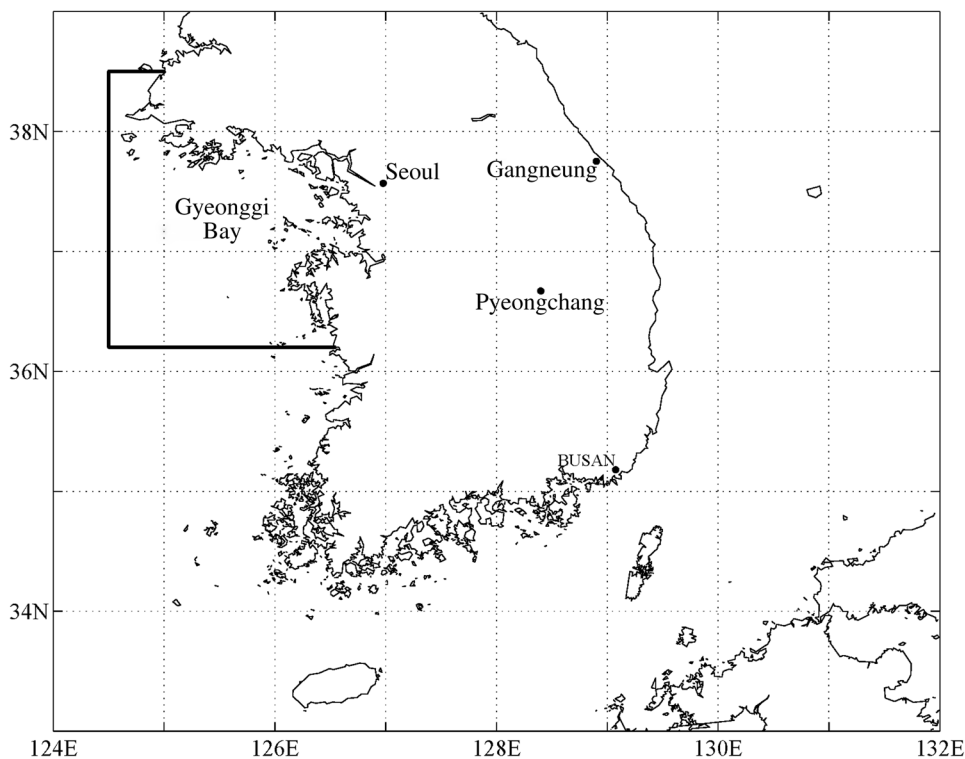


Fig. 1 The navy coastal ocean model (NCOM) model domain. The subdomain around the Gyeonggi Bay is the area where the analysis of Geostationary Ocean Color Imager (GOCI) images and the NCOM model currents was conducted.

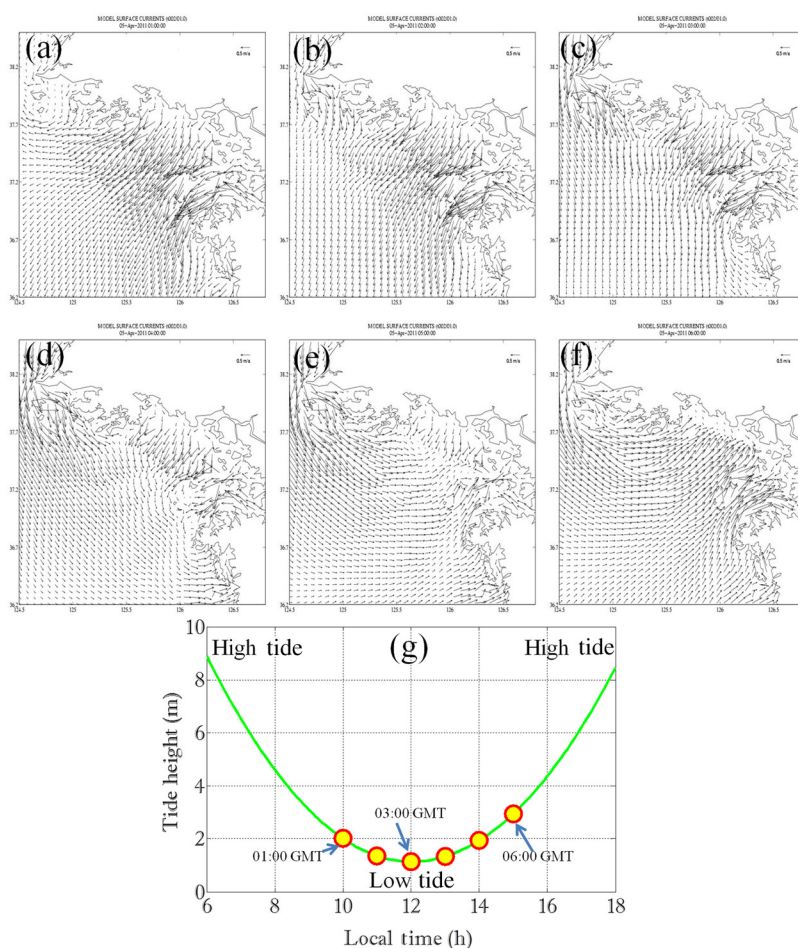


Fig. 2 NCOM predicted current around Gyeonggi Bay on April 5, 2011, at (a) 01:00 GMT, (b) 02:00 GMT, (c) 03:00 GMT, (d) 04:00 GMT, (e) 05:00 GMT and (f) 06:00 GMT. (g) The tidal data at Incheon (37.4667° N and 126.5833° E) acquired from, where high tide was 8.89 m at 6:08 am local time (sunrise at 6:14 am), low tide was 1.14 m at 12:17 pm local time, and high tide was 8.47 m at 6:17 pm local time (sunset at 6:59 pm).

the morning hours while in the afternoon hours it was flowing toward the coast. These tide-dominated waters usually carry significant amounts of SPM, which plays a major role in ocean health, particularly in coastal waters. SPM in the coastal waters of Korean Peninsula is relatively high ($>20 \text{ mg/m}^3$) and during winter it is particularly high ($>100 \text{ mg/m}^3$).⁴⁵ *In situ* measurements have shown that SPM can vary by a factor of 2 or more during the day due to horizontal advection and/or vertical resuspension forced by tides or wind events.^{46,47} Temporal frequency afforded by GOCI for the first time allows us to study these high temporal frequency variations in the water surface.

4 Results and Discussion

MODIS-aqua standard chlorophyll image for April 5, 2011, over the Korean Peninsula is shown in Fig. 3(a) while the corresponding standard GOCI chlorophyll image retrieved through the GDPS is shown in Fig. 3(d). In Figs. 3(a) and 3(d), the observed chlorophyll concentration is higher in the coastal regions, particularly along the western and southern parts of the Korean Peninsula. Yet this higher chlorophyll concentration may not represent true chlorophyll because chlorophyll-like features may arise from CDOM plumes, sediments plumes and bottom reflectance when using blue–green band ratio algorithms.^{13–16} Thus, in turbid waters, chlorophyll product is not adequate to identify bio-optical features. Instead, we used the FLH and the RBD

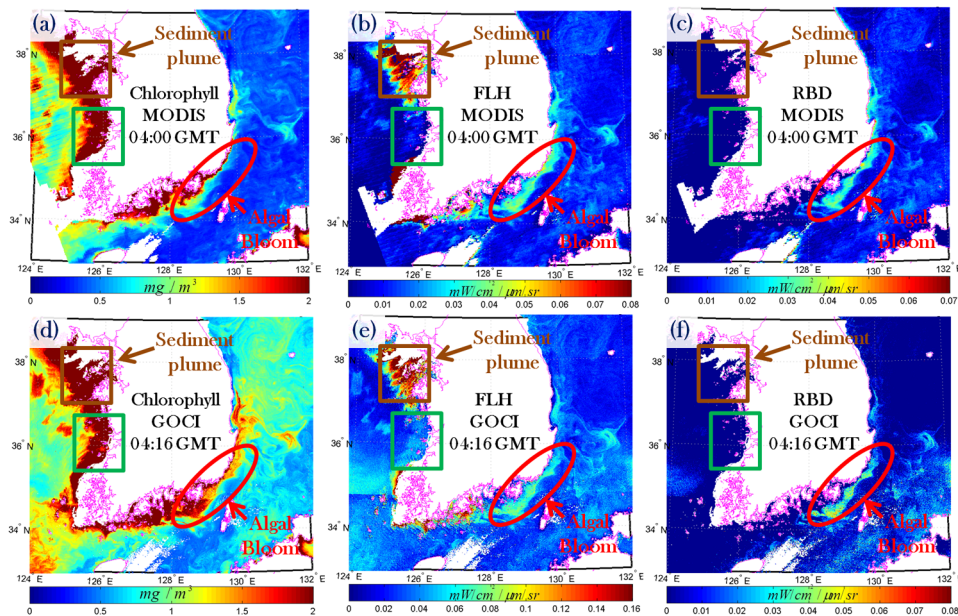


Fig. 3 MODIS ocean color products from April 5, 2011, acquired at 04:00 GMT: (a) chlorophyll image, (b) fluorescence line height (FLH) image, and (c) red band difference (RBD) image. GOCI ocean color products (data processed with GOCI data processing system GDPS) from April 5, 2011, acquired at 04:16 GMT, (d) chlorophyll image, (e) FLH image and (f) RBD image. Sediment rich region (red box), false high chlorophyll region (green box), and the algal bloom region (red circle).

for the surface features detection. Since FLH gives positive readings in both algae rich and sediment rich waters, while the RBD gives positive readings only in the algae rich waters,³ we can distinguish sediment rich waters from the algae rich waters by combining these approaches. An example is shown in Fig. 3, where Figs. 3(b) and 3(e) show the FLH images from MODIS and GOCI, respectively, while Figs. 3(c) and 3(f) show the RBD images from MODIS and GOCI, respectively. The features in the FLH images [Figs. 3(b) and 3(e)] are different from their respective chlorophyll images [Figs. 3(a) and 3(d)], particularly in the region shown with the green box. These false chlorophyll features are due to the aforementioned uncertainties associated with blue–green band ratio algorithms. Agreement between the features in MODIS and GOCI FLH images is much better than the corresponding chlorophyll images (Fig. 3). Uncertainties from imperfect atmospheric correction (which affects the blue/green wavelengths more strongly than the red/NIR wavelengths⁹), CDOM absorption, sediment absorption and bottom reflectance all explain why chlorophyll images have different features compared with FLH images. On the other hand, FLH overcomes most of these issues and provides more precise feature information from algal and nonalgal particles in the water surface. Since the water absorption is much stronger in the red–NIR regions, algorithms based on these spectral regions can only see the first few meters of the surface waters. However, for surface feature detection and monitoring purposes, this could be beneficial because interference from bottom reflectance will be reduced, unlike with blue–green algorithms. Even though the FLH has many advantages over the blue–green band ratio algorithms, it breaks down in highly scattering waters, where high red peak values in the reflectance are primarily due to contributions from elastic scattering modulated by chlorophyll absorption rather than the fluorescence, thus falsely indicating possible chlorophyll rich areas.^{48–50} In contrast, the RBD technique easily differentiates between the two effects, giving positive values under true bloom conditions and negative values in highly scattering waters.³ The RBD approach is for high chlorophyll concentration (>1 mg/m³) waters and it depends on the chlorophyll fluorescence quantum yield and the backscattering properties of the particles in the water.^{3,32} Corresponding RBD images are shown in Figs. 3(c) and 3(f) for MODIS and GOCI, respectively, where the agreement between the features in both images is very reasonable. Additionally, the sediment rich regions in the FLH images (brown box in Fig. 3) are no longer present in the RBD images. This is not surprising since FLH cannot

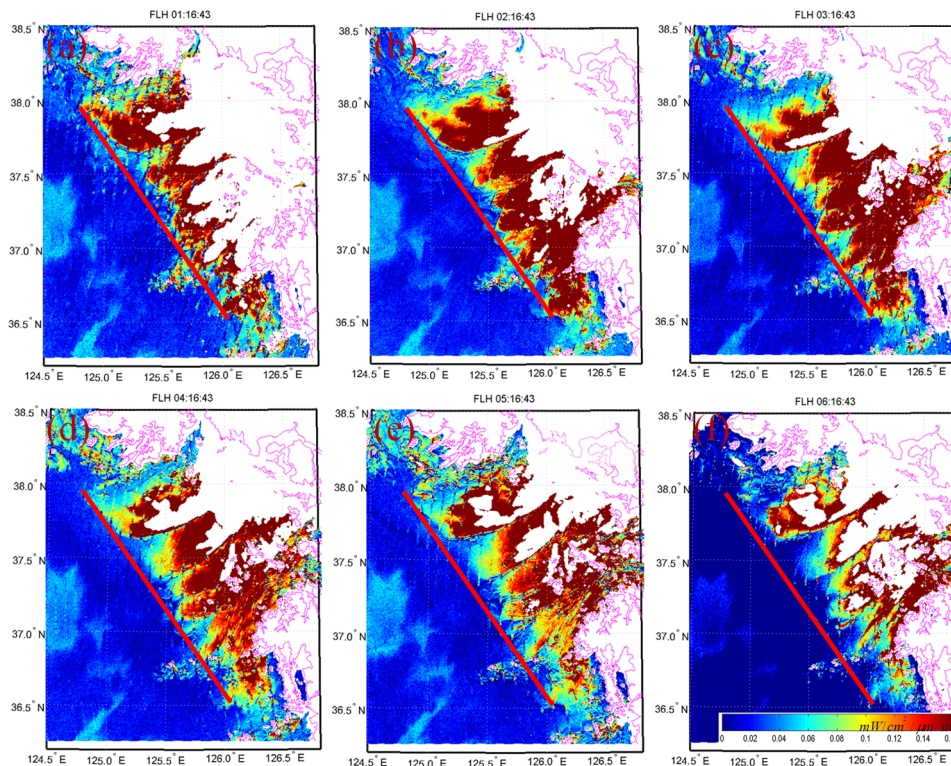


Fig. 4 GOCI FLH images around Gyeonggi Bay acquired on April 5, 2011, at (a) 01:16 GMT, (b) 02:16 GMT, (c) 03:16 GMT, (d) 04:16 GMT, (e) 05:16 GMT and (f) 06:16 GMT.

differentiate between sediment rich waters and chlorophyll rich waters, while the RBD only detects chlorophyll rich waters (red circle in Fig. 3). The RBD and FLH results (Fig. 3) are also consistent with our previous study based on the west coast of Florida.³ Since MODIS RBD and FLH results have been validated, we used MODIS to validate GOCI results. The GOCI image shown in Fig. 3 was acquired on April 5, 2011, at 04:16 GMT, which was approximately 16 min after the MODIS acquisition [Figs. 3(a)–3(c)]. Considering that data are from two different sensors and that they are processed through two different processing systems, the agreement between GOCI and MODIS results is very good for both FLH and RBD products. Note that the MODIS and GOCI scales differ slightly because MODIS and GOCI red bands are situated at slightly different wavelengths. MODIS red bands are about 11 nm apart (centered at 667 and 678 nm) while GOCI red bands are located about 20 nm apart (centered at 660 and 680 nm). Thus, GOCI values are slightly higher than the MODIS values.

To track sediment movement from the GOCI hourly images, we created hourly FLH images. Figure 4 shows the hourly (01:16 GMT to 06:16 GMT) GOCI FLH images where the area with warm colors (reds) indicates highly turbid water regions, while the cool colors (blues) indicate relatively clear water regions. Land, clouds, and invalid pixels are shown in white. The red line in the figure helps to visualize the movement of the sediment plumes, where the movement is more prominent in Fig. 4(f). This is because the tide was highest in this image [see Fig. 2(g)] compared with rest of the GOCI images shown in Fig. 4. During the acquisition of other GOCI images [Figs. 4(a)–4(d)], tidal transition was taking place, thus it was difficult to see the movement on still images. However, our careful examination of the FLH images (Fig. 4) and corresponding NCOM currents (Fig. 2) shows that they are consistent in terms of the features' movements, which suggest that the optical and bio-optical features' movements in this region are tide driven.

5 Conclusion

We show that the temporal frequency afforded by the GOCI sensor can be effectively used to detect and monitor temporal dynamics of the turbidity due to algal and nonalgal particles in

the surface waters. We successfully separate the regions with high algal and nonalgal particles from GOCI and validate the results with MODIS imagery. Good agreement between GOCI and MODIS also suggests that the GOCI sensor is capable of producing quality ocean color products. Additionally, sediment movement shown by hourly GOCI FLH images agrees well with the dynamics predicted by the NCOM model and with tidal data, demonstrating the importance of geostationary ocean color satellites.

Acknowledgments

This work is supported by the Center for the Advancement of Science in Space (CASIS) through NASA Cooperative Agreement No. NNH11CD70A.

References

1. J. K. Choi et al., "GOCI, the world's first geostationary ocean color observation satellite, for the monitoring of temporal variability in coastal water turbidity," *J. Geophys. Res.* **117**, c09004 (2012).
2. J. H. Ryu et al., "Overview of Geostationary Ocean Color Imager (GOCI) and GOCI data processing system (GDPS)," *Ocean Sci. J.* **47**(3), 223–233 (2012).
3. R. Amin et al., "Novel optical techniques for detecting and classifying toxic Dinoflagellate *Karenia brevis* blooms using satellite imagery," *Opt. Express* **17**(11), 9126–9144 (2009).
4. R. Amin et al., "MODIS and MERIS detection of dinoflagellates blooms using the RBD technique," *Proc. SPIE* **7473**, 747304 (2009).
5. M. J. Furnas, "In situ growth rates of marine phytoplankton: approaches to measurement, community and species growth rates," *J. Plankton Res.* **12**, 1117–1151 (1990).
6. H. R. Gordon and M. Wang, "Retrieval of water-leaving radiance and aerosol optical thickness over the oceans with SeaWiFS: a preliminary algorithm," *Appl. Opt.* **33**, 443–452 (1994).
7. D. A. Siegel et al., "Atmospheric correction of satellite ocean color imagery: the black pixel assumption," *Appl. Opt.* **39**(21), 3582–3591 (2000).
8. C. Hu, K. L. Carder, and F. E. Muller-Karger, "Atmospheric correction of SeaWiFS imagery over turbid coastal waters: a practical method," *Remote Sens. Environ.* **74**(2), 195–206 (2000).
9. R. Amin et al., "Impacts of atmospheric corrections on algal bloom detection techniques," in *Proc. Eighth Conf. on Coastal Atmospheric, Oceanic Prediction, Processes* (2009).
10. J. E. O'Reilly et al., "Ocean color chlorophyll a algorithms for SeaWiFS, OC2, and OC4: version 4," in *SeaWiFS Postlaunch Calibration and Validation Analyses, Part 3 SeaWiFS Postlaunch Technical Report Series*, S. B. Hooker and E. R. Firestone, Eds., pp. 9–23, NASA, Goddard Space Flight Center, Greenbelt, Maryland (2000).
11. H. R. Gordon et al., "Phytoplankton pigment concentrations in the middle Atlantic Bight: comparison of ship determinations and CZCS estimates," *Appl. Opt.* **22**, 20–36 (1983).
12. K. L. Carder et al., "Semi-analytic moderate-resolution imaging spectrometer algorithms for chlorophyll a and absorption with bio-optical domains based on nitrate-depletion temperatures," *J. Geophys. Res.* **104**, 5403–5422 (1999).
13. K. L. Carder et al., "Reflectance model for quantifying chlorophyll-a in the presence of productivity degradation products," *J. Geophys. Res.* **96**(C11), 20599–20611 (1991).
14. D. A. Siegel et al., "Colored dissolved organic matter and its influence on the satellite-based characterization of the ocean biosphere," *Geophys. Res. Lett.* **32**(20), L20605 (2005).
15. A. Morel and B. Gentili, "The dissolved yellow substance and the shades of blue in the Mediterranean Sea," *Biogeosciences* **6**(11), 2625–2636 (2009).
16. A. Brown et al., "The origin and global distribution of second order variability in satellite ocean color and its potential applications to algorithm development," *Remote Sens. Environ.* **112**(12), 4186–4203 (2008).
17. G. Neukermans et al., "Mapping total suspended matter from geostationary satellites: a feasibility study with SEVIRI in the southern North Sea," *Opt. Express* **17**, 14029–14052 (2009).

18. J. H. Ryu et al., "Temporal variation in Korean coastal waters using Geostationary Ocean Color Imager," *J. Coastal Res.* **64**, 1731–1735 (2011).
19. NASA LAADS Web, "Level 1 and Atmosphere Archive and Distribution System," www.ladsweb.nascom.nasa.gov (June 2013)
20. H. J. Han, J. H. Ryu, and Y. H. Ahn, "Development of Geostationary Ocean Color Imager (GOCI) data processing system (GDPS)," *Korean J. Remote Sens.* **26**(2), 239–249 (2010).
21. H. J. Han et al., "Preliminary verification results of the geostationary ocean color satellite data processing software system," *Proc. SPIE* **7861**, 786108 (2010).
22. P. Martinolich and T. Scardino, "Automated processing system User's Guide Version 4.2," 2011, http://www7333.nrlssc.navy.mil/docs/aps_v4.2/html/user/aps_chunk/index.xhtml (May 2013)
23. P. J. Martin, "Description of the navy coastal ocean model version 1.0," Report NRL/FR/732-00-9962, Navy Research Laboratory, Stennis Space Center, Mississippi (2000).
24. R. C. Rhodes et al., "Navy real-time global modeling systems," *Oceanography* **15**(1), 29–43 (2002).
25. C. N. Barron et al., "Formulation, implementation and examination of vertical coordinate choices in the global navy coastal ocean model (NCOM)," *Ocean Model.* **11**(3–4), 347–375 (2006).
26. T. E. Rosmond et al., "Navy operational global atmospheric prediction system (NOGAPS): forcing for ocean models," *Oceanography* **15**, 99–108 (2002).
27. G. D. Egbert and S. Y. Erofeeva, "Efficient inverse modeling of barotropic ocean tides," *J. Atmos. Oceanic Technol.* **19**, 183–204 (2002).
28. J. Cummings et al., "Ocean data assimilation systems for GODAE," *Oceanography* **22**(3), 96–109 (2009).
29. J. Cummings, "Operational multivariate ocean data assimilation," *Q. J. R. Meteorol. Soc.* **131**, 3583–3604 (2005).
30. I. Shulman et al., "Impact of glider data assimilation on the Monterey Bay model," *Deep Sea Res. Part II*, **56**, 128–138 (2009).
31. I. Shulman et al., "Observed and modeled bio-optical, bioluminescent, and physical properties during a coastal upwelling event in Monterey Bay, California," *J. Geophys. Res.* **116**, C01018, (2011).
32. R. Amin, B. Penta, and S. Derada, "Occurrence and extent of HABs on the West Florida Shelf 2002-present," *IEEE Geosci. Remote Sens. Lett.* (2015).
33. R. Amin, "Optical algorithms for assessment of fluorescence sources in sea waters," PhD Thesis, Univ. of New York (2009).
34. I. M. Soto Ramos, "Harmful Algal Blooms of the West Florida Shelf and Campeche Bank: visualization and quantification using remote sensing methods," PhD Thesis, Univ. of South Florida (2013).
35. Y. W. Lee and G. Kim, "Linking groundwater-borne nutrients and dinoflagellate red-tide outbreaks in the southern sea of Korea using a Ra tracer," *Estuarine Coastal Shelf Sci.* **71**, 309–317 (2007).
36. C. H. Kim, T. G. Park, and C. Lee, "Harmful dinoflagellates and mitigation strategies in Korea," *Philipp. J. Sci.* **139**(2), 139–147 (2010).
37. Y. W. Lee et al., "A relationship between submarine groundwater-borne nutrients traced by Ra isotopes and the intensity of dinoflagellate red-tides occurring in the southern sea of Korea," *Limnol. Oceanogr.* **55**(1), 1–10 (2010).
38. R. M. Letelier and M. R. Abbott, "An analysis of chlorophyll fluorescence algorithms for the moderate resolution imaging spectrometer (MODIS)," *Remote Sens. Environ.* **58**, 215–223 (1996).
39. C. S. Kim et al., "Residual flow and its implication to macro-tidal flats in Kyunggi Bay estuary of Korea," *J. Coastal Res.* **56**, 976–980 (2009).
40. H. J. Lee, U. H. Kim, and Y. S. Chu, "Sedimentology of tidal flats on the west coast, Korea," *Ocean Res.* **20**(2), 153–165 (1998).
41. H. J. Woo, S. K. Chang, and Y. S. Chu, "Recent foraminifera and surface sediments in tidal flats of the west coast of Korea," *Ocean Res.* **20**(2), 63–72 (1998).

42. H. J. Woo and J. G. Je, "Changes of sedimentary environments in the southern tidal flat of Kanghwa island," *Ocean Polar Res.* **24**(4), 331–343 (2002).
43. C. S. Kim and H. S. Lim, "Sediment dispersal and deposition due to sand mining in the coastal waters of Korea," *Cont. Shelf Res.* **29**(1), 194–204 (2009).
44. Mobile Geographics LLC, "Live marine information," www.sailwx.info (June 2014).
45. Y. K. Choi and J. N. Kwon, "Seasonal variation of transparency in the southeastern Yellow Sea," *J. Korean Fish.* **31**(3) 323–329 (1998).
46. D. Eisma and G. Irion, "Suspended matter and sediment transport," in *Pollution of the North Sea: An Assessment*, W. Salomons et al., Eds., pp. 20–33, Springer, Berlin (1988).
47. C. E. L. Thompson et al., "In situ flume measurements of resuspension in the North Sea," *Estuarine Coastal Shelf Sci.* **94**(1), 77–88 (2011).
48. A. Gilerson et al., "Fluorescence component in the reflectance spectra from coastal waters. Dependence on water composition," *Opt. Express* **15**(24), 15702–15721 (2007).
49. A. Gilerson et al., "Fluorescence component in the reflectance spectra from coastal waters. II. Performance of retrieval algorithms," *Opt. Express* **16**(4), 2446–2460 (2008).
50. D. McKee et al., "Potential impacts of nonalgal materials on water-leaving Sun induced chlorophyll fluorescence signals in coastal waters," *Appl. Opt.* **46**(31), 7720–7729 (2007).

Ruhul Amin received his BE degree in computer engineering and the ME degree in electrical engineering from the City College of New York, New York, NY, USA, in 2005 and 2008, respectively, and the MPhil and PhD degrees in electrical engineering from the City University of New York, NY, USA, in 2008 and 2009, respectively. Since 2015, he has been the chief scientist with the BioOptoSense LLC. He has developed optical algorithms to detect harmful algal blooms, cloud-shadows, and sea-ice. His current research interests include optical algorithm development, atmospheric corrections, cloud-shadows, sea-ice, fluorescence, and harmful algal blooms.

Igor Shulman is oceanographer with the Naval Research Laboratory at Stennis Space Center. He received his PhD in mechanics of fluid, gas, and plasma from the Moscow University of Oil and Gas Technology in 1982. He has been PI and Co-PI on numerous interdisciplinary projects funded by ONR, NOPP, and MURI. His research interests are in modeling of physical and bio-optical oceanic processes, data assimilation, and analysis of observations. He has published 74 articles in refereed journals in English and in Russian.